Transportation Infrastructure Geotechnology (2024) 11:3424–3450
https://doi.org/10.1007/s40515-024-00416-4

TECHNICAL PAPER

Influence of Geosynthetic Reinforcement Geometrical Parameters on Load-Bearing Capacity of Sand: An Experimental Study

Venkatesh Buragadda[1,3] · T. Thyagaraj[2] · Rishav Dhiman[2] · Eswara Reddy Orekanti[1] · Tharun Kumar Maddileti[1]

Accepted: 13 May 2024 / Published online: 28 May 2024

Abstract

The aim of this research is to increase the load-carrying capacity of the geotextile-reinforced soils by making a series of modifications to the reinforcement. Laboratory model tests with various types of geosynthetics are evaluated: plane geotextile, grid-geotextiles with a common rib size but having different apertures, grid-geotextiles with varying rib sizes having an optimal aperture, and biaxial geogrid reinforcement layers. Irrespective of aperture and rib sizes, the tensile strength and stiffness of the grid-geotextile reinforcement layers were 2 times lower in comparison to the plane geotextile. In spite, the plate load test results revealed that the sand bed reinforced with low tensile strength and stiffness of grid-geotextile showed 1.15 times improvement as settlement ratio enhanced in comparison to sand bed reinforced with high tensile strength and stiffness of plane geotextile. This improvement is attributed to the interface and interlocking mechanism of the grid-geotextile reinforcement layers. The test results of grid-geotextile and biaxial geogrid-reinforced sand beds are compared. Also, this paper highlighted the influence parameters of geogrid reinforcements and accentuated their optimum ranges to the acquisition of maximum reinforcement benefits. Simple correlations were developed and presented along with the limits for the determination of the bearing capacity ratio of geogrid-reinforced sand beds with the influencing factors.

Keywords Laboratory model tests · Sand · Geosynthetics · Grid-geotextile reinforcement · Bearing capacity

Extended author information available on the last page of the article

1 Introduction

Reinforced soil is a technique that strengthens the soil by including reinforcement materials such as geotextiles, geogrids, geo-composites, and geocells (Shukla et al. 2009). The effect of geogrid reinforcements on soil load-carrying capacity has been studied by various researchers such as Sitharam and Sireesh (2004), Brown et al. (2007), Latha and Somwanshi (2009a, 2009b), and Useche-Infante et al. (2019), while a few researchers examined the effect of geotextile and geo-composite reinforcements on soil load-carrying capacity, e.g., Hsieh and Mao (2005), Brown et al. (2007), Tafreshi and Dawson (2010), Abu-Farsakh et al. (2013), and Buragadda and Thyagaraj (2019). The improved load-carrying capacity of the reinforced sand bed depends on the mechanism of the reinforcement materials such as the frictional resistance mechanism (geotextiles) and passive resistance mechanism (geogrids) (Guido et al. 1986; Guo et al. 2020). Moreover, in the case of geogrid-reinforced soils, various parameters influenced the effect of reinforcement on soil load-carrying capacities, such as soil properties, reinforcement properties, and foundation properties (e.g., footing size, shape, and embedment depth) (Hsieh and Mao 2005; Mehrjardi and Khazaei 2017). Brown et al. (2007) reported that the influence of aspect ratio, i.e., the ratio of aperture size to the medium soil grains size (D_{50}), plays a significant role in the improvement of soil load-bearing capacity in comparison to the reinforcement physical and mechanical properties such as the geometry of apertures, tensile strength, and junction strength (Gongora and Palmeira 2016). Also, they found the optimum ranges of the influencing parameters in different ratio forms such as D/d_{min}, D/D_{50}, and d_{min}/D_{50} by conducting the model tests under repeated loading conditions (Brown et al. 2007). However, all these studies are limited to cyclic loading and no studies for the cases of monotonic or static loading conditions.

Literature shows that the load-carrying capacity of the sand beds improved extensively with the geogrid reinforcement layers rather than the geotextile reinforcements for the same reinforcement quantity (Guido et al. 1986; Hsieh and Mao 2005; Abu-Farsakh et al. 2013). According to the authors' cost observations, the sand beds reinforced with geogrid layers are more costly than the geotextile reinforcement layers because the unit area cost of the geogrid layer is 3.5 times more expensive than the same quantity of geotextile. Apertures present in the geogrid reinforcement layers exhibit 1.12 times higher load-carrying capacity improvement than the geotextile reinforced sand and 1.63 times higher in comparison with unreinforced soils (Guido et al. 1986; Abu-Farsakh et al. 2013). Besides mobilizing the frictional mechanism in geotextile reinforcement layers, it is possible to mobilize the interlocking mechanism in geotextile reinforcement layers, such as the geogrid reinforcement layer, by creating small openings through punching.

Therefore, the present study attempts to utilize the interlocking contribution of geotextile layers in improving the load-bearing capacity of geotextile-reinforced sand beds by providing apertures (i.e., small openings) in the geotextile reinforcements. The geotextile prepared with apertures is hereafter called

"grid-geotextile." This paper presents the effect of the size of the apertures and ribs of the reinforcement layer on improving the sand load-carrying capacity based on laboratory model tests using grid-geotextile. Then, the effect of the grid-geotextile reinforcement layer on load-carrying improvement was compared with the results of plane geotextile and commercially available geogrid reinforcement layer sand beds.

2 Material Properties

2.1 Sand

The laboratory model tests were performed using clean and dry sand, which was collected locally from Chennai's surrounding areas and grain size distribution (ASTM D6913 2017) is presented in Fig. 1. Based on Fig. 1, the test soil consists of a higher percentage of sand-size particles, i.e., < 4.75 mm size and according to the Unified Soil Classification System (USCS), the soil is classified as poorly graded sand (represented by "SP"). Table 1 presents the physical properties of the soil used in the present study. The model tests in the present study were performed by placing the sand bed at a relative density of 70%. The sand shear strength properties of the angle of internal friction (ϕ) and cohesion at the respective relative density (R_d) of 70% were found as 40.20° and 0 kPa by performing tests using standard small size (60 mm × 60 mm × 25 mm) direct shear test apparatus.

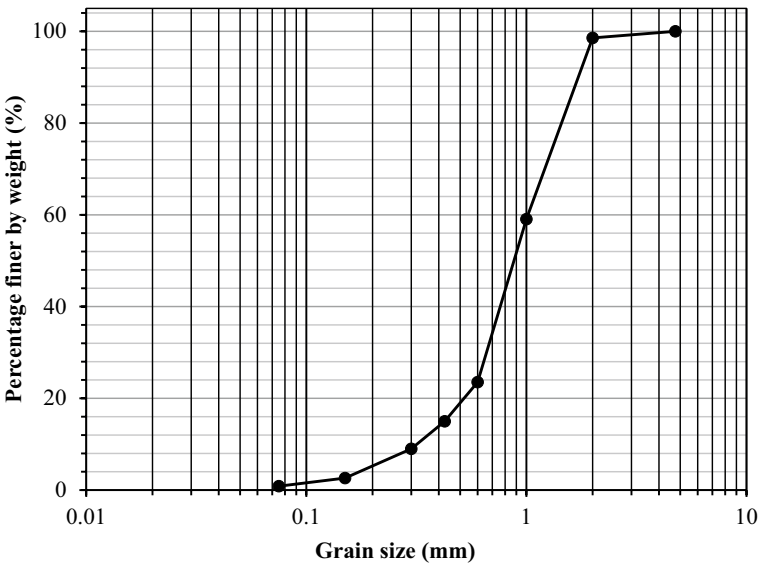

Fig. 1 Particle size distribution curve of sand

Table 1 Properties of test sand used in the present research

Properties	Value
Specific gravity, G_s	2.69
Grain size distribution (%)	
Gravel	0
Sand	97.4
Fines	2.6
D_{10} (mm)	0.33
D_{30} (mm)	0.67
D_{50} (mm)	0.90
D_{60} (mm)	0.86
C_u	3.03
C_c	1.36
Unified soil classification symbol (USCS)	SP
Maximum dry unit weight (kN/m^3)	17.96
Minimum dry unit weight (kN/m^3)	15.80
Dry unit weight corresponding to 70% relative density (kN/m^3)	17.25
Shear strength parameters at 70% relative density	
Angle of internal friction, ϕ (°)	40.20°
Cohesion (kPa)	0

2.2 Reinforcement Materials

2.2.1 Geotextile and Geogrid

The model tests are performed on the sand bed reinforced with synthetic polypropylene geotextile (PPGT) and synthetic polypropylene biaxial geogrid (GG) reinforcement layers. The polypropylene geotextile (Techno Fabric TF–41) was collected from Techno Fabrics Geosynthetic (P) Ltd., Gujarat, India. The polypropylene biaxial geogrid (Strata Grid SG–40) was collected from Strata Geosystems (P) Ltd., Mumbai, India. The photographic view of the geotextile (TF–41) and geogrid (SG–40) is shown in Fig. 2. The physical and mechanical properties of the TF–41 and SG–40 are determined according to ASTM Standard as presented in Table 2.

2.2.2 Grid-geotextile

To generate the interlocking effect in the geotextile, the openings are systematically made along the machine direction (MD) and cross-machine direction (CMD) of the geotextile layer. The openings were made on the geotextile with the help of an electrical soldering rod. The synthetic geotextile for the model tests was made with a polymer substance of polypropylene group, which can be moldable in the presence of heat. Therefore, the synthetic polypropylene geotextile was punched in the presence of heat, which can be produced by the tip of the soldering rod with a supply of electrical current. To evaluate the effect of aperture size and rib width of the

(a) (b)

Fig. 2 Photographic view of the different types of geosynthetics used in the present study: **a** PPGT: TF–41; **b** GG: SG–40

grid-geotextile on the improvement of the load-carrying capacity of the reinforced sand bed, different types of grid-geotextiles with various aperture sizes were prepared for the present model tests as presented in the photographic view in Fig. 3. Similarly, grid-geotextiles with 10 mm × 10 mm aperture size having various rib sizes were prepared for the present model tests. Based upon the aperture size (represented by "*G*") and rib size (represented by "*R*") of grid-geotextile, the reinforcement is called G10R15, G20R15, G30R15, G10R25, and G10R35. The tensile test properties of the grid-geotextiles of both machine direction (MD) and cross-machine direction (CMD) were determined using the wide-width tensile test method as per ASTM Standard D4595-17 (2017). The properties of the grid-geotextile are summarized in Table 2. The tensile stress–strain behavior of geosynthetic reinforcements used in the present study is depicted in Fig. 4.

3 Description of Laboratory Model Tests

3.1 Experimental Test Setup

The experimental model tests are conducted in the laboratory using a steel tank with inner dimensions of length (*L*) × width (*B*) × depth (*h*) 1000 mm × 1000 mm × 1000 mm, respectively. The rigid steel plate with a 25 mm thickness and a circular shape of 150 mm diameter (*D*) was used as a model footing. The maximum loading plate sizes comply based on the test tank dimensions (i.e., 5–6*D*) to eliminate the side boundaries effect while loading application on the footing (Latha and Somwanshi, 2009a, 2009b). Generally, the footing in in situ conditions has a rough surface at the interface of the foundation material and footing base. Therefore, to replicate the rough nature of the footing base, a thin layer of sand was

Table 2 Properties of geosynthetics

Property	Standards	TF–41	SG–40	Grid-geotextile				
				Aperture effect (*G*)		Rib effect (*R*)		
Physical property		PPGT	PPGT	G10R15	G20R15	G30R15	G10R25	G10R35
Aperture shape		NA	Rectangle	Rectangle	Rectangle	Square	Square	Square
Aperture size—MD × CMD (mm)		NA	20 × 17	10 × 10	20 × 17	30 × 30	10 × 10	10 × 10
Rib size—MD × CMD (mm)		NA	2 × 1	15	15	15	25	35
Thickness (mm)	ASTM D5199-12 (2012)	0.4	0.6	0.4	0.4	0.4	0.4	0.4
Mass per unit area (g/m^2)	ASTM D5261-10 (2018)	130	413	126	111	94	128	130
Ratio of $\frac{d_{min}}{D_{50}}$		NA	18.88	10.00	18.88	33.33	10.00	10.00
Mechanical property								
Ultimate tensile strength—MD × CMD (kN/m)	ASTM D4595-17 (2017) and ASTM D6637-15 (2015)	29.6 × 23.5	42.9 × 41.9	10.93 × 4.25	8.47 × 3.77	4.74 × 3.97	11.67 × 11.33	12.7 × 12.67
Failure strain—MD × CMD (%)		30.2 × 21.4	27 × 24	18.6 × 15.2	22.7 × 18.6	25.2 × 20.1	19 × 21	20.6 × 20.2
Secant modulus (tensile stiffness), *EA* at 5% strain (kN/m)		101	181	33	13	6	52	58

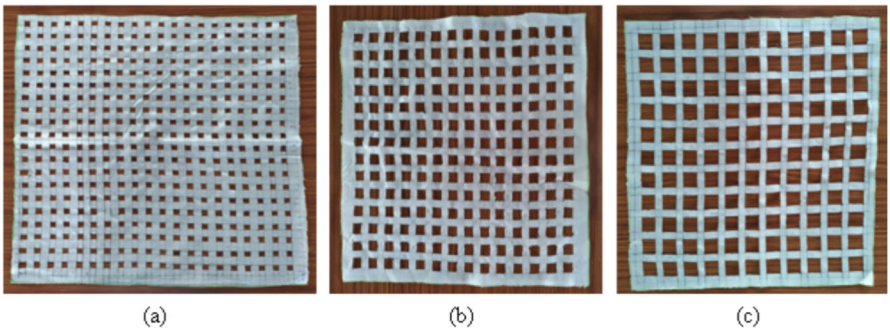

Fig. 3 Photograph of the different aperture sizes of grid-geotextiles used in the present study: **a** G10R15, **b** G20R15, **c** G30R15

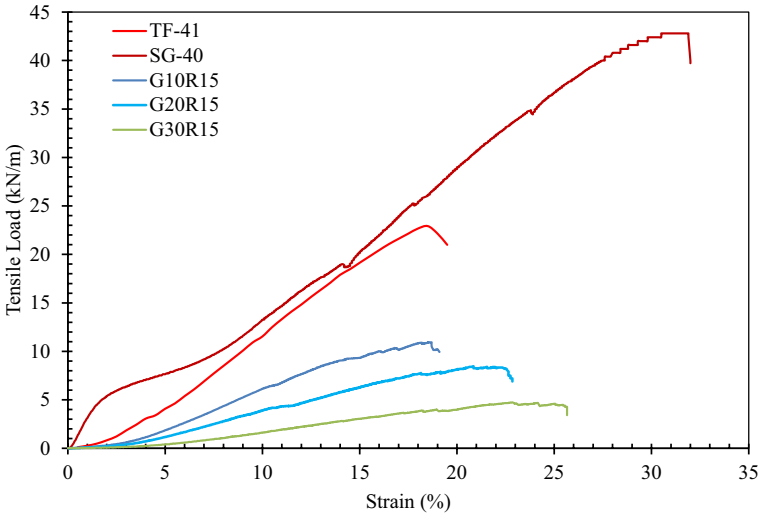

Fig. 4 Tensile stress–strain behavior of different geosynthetic materials (only M-direction)

attached to the base of the footing plate with the help of epoxy glue. To eliminate the eccentricity of loading, the footing was placed precisely at the center of the test tank, and the load application on the footing was applied through the hand-operated hydraulic jack. Figure 5 presents the photographic view of the total test setup.

3.2 Sand Bed Preparation for the Laboratory Model Tests

The model tests were conducted in the present study using the rainfall technique. A small steel tank with inner dimensions of 400 mm (L)×400 mm (B)×300 mm (h) was used to determine the effect of sand height of fall on its relative density (R_d). Initially, the sand was poured into the steel tank at some height of fall, and

Fig. 5 Photograph of experimental setup

once the tank was filled with the poured sand, the amount of sand collected inside the tank was then measured with the help of a weighing machine with an accuracy of 0.01 g. The accumulated sand unit weight inside the tank was calculated from the known volume, i.e., 0.071 m^3. Based on the maximum and minimum dry unit weights of the sand as presented in Table 1, the sand relative density was calculated. A similar procedure was followed and calculated sand relative density (R_d) at different heights of fall (h_f). The relationship between the sand relative density and respective height of fall (h_f) was presented in a graphical plot. The height of fall (h_f) corresponding to the desired relative density (R_d) of sand can easily be determined from the graphical plot and used for preparing the sand bed in the steel tank of 1000 mm × 1000 mm × 1000 mm. For the present laboratory model tests, the relative density of sand is fixed as 70% (i.e., dry unit weight = 17.23 kN/m^3). The sand placement density while preparing the sand bed was checked by placing small aluminum cups at different locations in the test tank (Buragadda and Thyagaraj 2019).

3.3 Reinforcement Layout and Preparation for the Model Tests

The synthetic polypropylene plane geotextile and different types of grid-geotextiles and geogrid were used for the present model tests. In each model test, the

geometrical parameters of the placement depth of the first reinforcement layer, consequent spacing between the reinforcement layers, the number of reinforcement layers, and the size of the reinforcement layer are denoted as "u," "h," "N," and "B_r." The reinforcement geometrical parameters of "u," "h," and "B_r" are normalized with the footing diameter (D) and expressed in a non-dimensional form as $\frac{u}{D}$, $\frac{h}{D}$, and $\frac{B_r}{D}$ (Latha and Somwanshi 2009a, 2009b).

4 Experimental Procedure

Irrespective of unreinforced and reinforced sand bed conditions, the model tests conducted on a sand bed with 1000 mm depth were prepared by adopting an air-pluviation technique inside the test tank of 1000 mm × 1000 mm × 1000 mm. While preparing the sand bed in unreinforced condition, sand was poured continuously inside the test tank without ceasing (except for placement density crosscheck). Further, in the case of conducting model tests on reinforced sand beds, the sand pluviation technique stopped at every interval of reinforcement layer layout placement depths inside the test tank. Once the sand reached the reinforcement layer layout placement depth, the sand pouring technique stopped and the sand surface was leveled properly using a small wood plank and checked with a level tube by placing it at various locations in the test tank. Once the tank was filled up to the 1000-mm desired depth, the footing was placed exactly at the center of the test tank and below the loading jack. The loading was applied on the footing with the help of a hand-operated hydraulic jack through the ball-bearing arrangement. The ball-bearing arrangement helped distribute the vertical loads centrically and vertically during loading application on the footing. The load was applied incrementally using a pre-calibrated proving ring as per the protocol of IS 1888–1982 (1982). Each load increment was maintained until the footing settlement stabilized (i.e., less than 0.02 mm/min). As shown in Fig. 5, the footing settlements are measured with dial gauges named D_1 and D_2, respectively. The dial gauges D_1 and D_2 can move each up to 50 mm with the least count of 0.01 mm accuracy. For reliability on the consistency of test results, most of the model tests are performed repeatedly two to three times, despite the ratio of footing size (D) to the medium size of soil particles (D_{50}) being more than four times a factor of the limit proposed by Hsieh and Mao (2005). The test results of load-settlement characteristics of sand in all trails are close match only with the variance of around 8%.

4.1 Experimental Program

A series of laboratory model tests was performed in the present study as summarized in Table 3. Initially, test Series A describes the model test carried out on an unreinforced sand bed (represented by URS). Series B model tests were conducted on synthetic plane polypropylene geotextile (TF–41) and biaxial geogrid (SG–40)-reinforced sand beds. To get the maximum improvement in the load-carrying capacity of the sand bed, the geometrical parameters of the reinforcement layers such as $\frac{u}{D}$, $\frac{h}{D}$,

Table 3 Details of laboratory model test series

Series designation	Geometrical parameters of reinforcement layers		Objective of the series
	Variable	Constant	
A	NA	NA	Tests on unreinforced sand
B		$\frac{u}{D}$= 0.3	For determination of the effect of geotextile and geogrid reinforcement layers on the load-bearing capacity
	TF–41	$\frac{h}{D}$= 0.3	
	SG–40	N= 4	
		$\frac{B_t}{D}$= 5	
C	Grid-geotextile *G*	$\frac{u}{D}$= 0.3	For determination of the effect of the aperture size (*G*) of the reinforcement layer on the load-bearing capacity
	G10R15	$\frac{h}{D}$= 0.3	
	G20R15	N= 4	
	G30R15	$\frac{B_t}{D}$= 5	
D	Grid-geotextile *R*	$\frac{u}{D}$= 0.3	For determination of the effect of the rib width (*R*) of the reinforcement layer on load-bearing capacity
	G10R15	$\frac{h}{D}$= 0.3	
	G10R25	N= 4	
	G10R35	$\frac{B_t}{D}$= 5	

N, and $\frac{B_r}{D}$ were maintained at optimum conditions of $\frac{u}{D} = 0.3$ (i.e., 46.5 mm), $\frac{h}{D} = 0.3$ (i.e., 45 mm), $N = 4$, and $\frac{B_r}{D} = 5$ (i.e., 750 mm), as recommended by Buragadda and Thyagaraj (2019). Buragadda and Thyagaraj (2019) found the optimum geometrical parameters using jute geotextile reinforcements and found the optimum width of reinforcement as 3.5 D. The improvement of the load-carrying capacity of reinforced sand beds drastically varies with reinforcement number (N) and size (B_r). Also, different mechanisms (i.e., strain restraining mechanism and wide-slab mechanism) are formed depending on the reinforcement size (Buragadda and Thyagaraj 2019; Guo et al. 2020). Whereas for achieving maximum load improvement, the required optimum width of geogrid reinforcements is less than that of geotextile reinforcements due to differences in the reinforcement's mechanism (Guido et al. 1986). However, based on the safety consideration point of view, irrespective of the type of reinforcement, the optimum width of reinforcement (B_r) is maintained as 5 D (i.e., > 3.5 D). As per Omar et al. (1993), the significant depth or critical depth of reinforced sand bed varies only based on the type of footing (i.e., strip and square/circular/rectangular). As per the literature, most of the test results showed the optimum depth of the reinforcement zone is only varied between 1.2 and 1.25 D, i.e., corresponding $N = 4$ (Buragadda and Thyagaraj 2019; Guido et al. 1986). Similarly, irrespective of the type of reinforcement, most of the test results show that the optimum geometrical parameters of u/D and h/D vary from 0.3 to 0.4 D (Guo et al. 2020). Hence, the optimum reinforcement geometrical parameters (i.e., u/D, h/D, and N) are maintained in the same way as recommended by Buragadda and Thyagaraj (2019). Series C tests were performed on a sand bed reinforced with three different types of grid-geotextile of varying aperture sizes (represented by G) in both the machine and cross-machine direction of the reinforcement layer. In Series C, the rib (i.e., the strip between the two apertures) width of the grid-geotextile was maintained the same in all the tests. The effect of the grid-geotextile with different rib widths is evaluated by conducting the laboratory model tests designated as Series D tests. In series D tests, three grid-geotextiles of different tensile strengths and rib widths (represented by R) were used. However, the aperture size (G) was maintained constant about an optimum condition obtained from the Series of C tests. Irrespective of the type and tensile strength of the grid-geotextile layer, the reinforcement layers were also placed at the optimum conditions as used in Series B tests.

5 Results and Discussion

In the case of reinforced soils, the improvement of the load-bearing capacity with the inclusion of reinforcements is represented by a term known as bearing capacity ratio (BCR). BCR is the ratio of reinforced soil load-carrying capacity (q_{rs}) to the unreinforced soil load-carrying capacity (q_{us}) at the same settlements. However, the ultimate load-carrying of unreinforced soil (q_{uult}) is used as q_{us} while determinations of BCR at higher settlements, i.e., > q_{uult}.

5.1 Comparison of Behavior of URS, TF–41-, and SG–40-Reinforced Sand Beds

As aforesaid, Series A and Series B model tests were conducted on unreinforced (URS), polypropylene geotextile (TF–41)-, and biaxial geogrid (SG–40)-reinforced sand beds. Figure 6 compares the load-settlement curves of URS, TF–41-, and SG–40-reinforced sand beds. The load-settlement behavior of the URS shows a peak value, while the load-settlement curves of TF–41- and SG–40-reinforced sand beds do not exhibit any peak. Also, the load-settlement behavior of the reinforced sand beds shows a higher improvement in load-bearing capacity than the URS. Further, the load-carrying capacity of SG–40 (geogrid)-reinforced sand bed is greater than the load-carrying capacity of TF–41 (geotextile) reinforcement sand, irrespective of the settlement of the footing. The variation of bearing capacity ratio (BCR) of TF–41- and SG–40-reinforced sand bed with footing settlement up to *s/D* of 12% is shown in Fig. 7. It could be observed from Fig. 7 that the load-carrying capacity of the SG–40-reinforced sand beds improved significantly in comparison to the load-carrying capacity of TF–41-reinforced sand beds, irrespective of footing settlement. For both TF–41- and SG–40-reinforced sand beds, the geometrical parameters such as *u/D*, *h/D*, *N*, and B_r/D of the reinforcement layer were maintained the same. Despite this, the improvement in the load-carrying capacity of the sand bed reinforced with SG–40 was higher. It is attributed to the higher reinforcement tensile stiffness (*EA*) and interlocking of sand particles through the aperture of the geogrid (SG–40) reinforcement layers as per Table 2 (Hsieh and Mao 2005; Abu-Farsakh

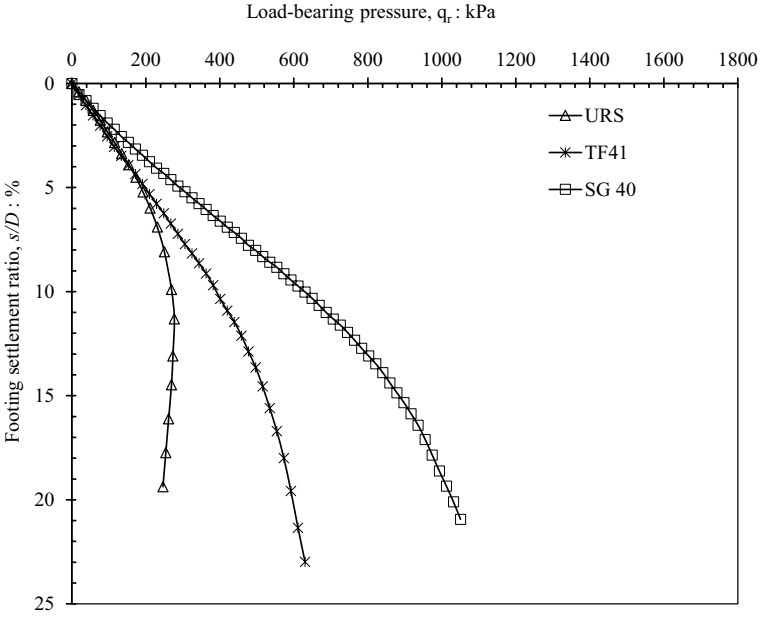

Fig. 6 Load-settlement response of URSD and reinforced sand with TF–41 and SG–40 reinforcement layers ($\frac{u}{D} = 0.3$, $\frac{h}{D} = 0.3$, $N = 4$, $\frac{B_r}{D} = 5$)

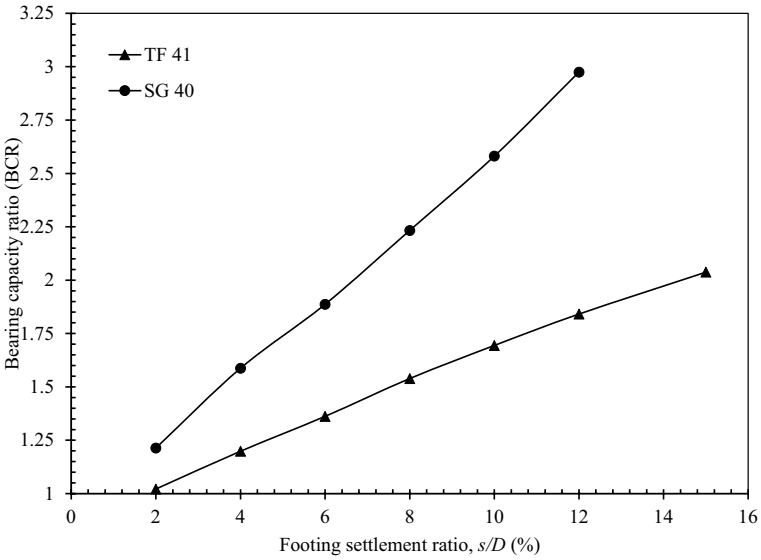

Fig. 7 Comparison of variation of the BCR of TF–41 and SG–40 reinforced sand for different footing settlements

et al. 2013; Guido et al. 1986). Therefore, the size of the aperture in the geogrid reinforcement plays a significant role.

5.2 Behavior of Grid-Geotextile–Reinforced Sand Beds

5.2.1 Effect of Aperture Size (G)

Series C model tests show the effect of the aperture size (represented by G) of the reinforcement on the load-carrying capacity of reinforced sand beds. Three grid-geotextiles with constant rib width (represented by R) but different aperture sizes were prepared and used for the plate load tests. Figure 8 compares the load-settlement behavior of the URS and sand bed reinforced with grid-geotextiles of different G. Figure 9 presents the variation of the bearing capacity ratio (BCR) with footing settlement ratio (s/D) of the sand bed reinforced with grid-geotextile of different aperture sizes of G. From Fig. 8, irrespective of the reinforcement G, the load-carrying capacity of the sand bed increased with increase in the footing settlement ratio (s/D).

It is evident from Fig. 9 that the BCR of the sand bed decreases with the increase in the aperture size (G) of the reinforcement layer. Furthermore, at larger G (i.e., G20R15 and G30R15), the BCR of reinforced sand bed at lower settlements (i.e., $s/D < 3\%$) is lesser than 1, which means that the load-carrying capacity of reinforced sand bed is much less in comparison to the unreinforced sand bed. It is primarily due to a lack of sufficient overburden pressure (i.e., u/D and h/D) with increasing

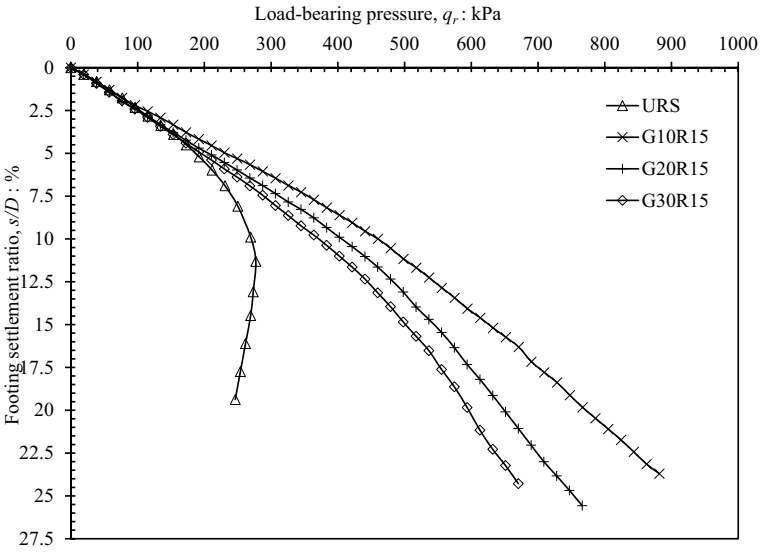

Fig. 8 Variation of the load-settlement curves of the URS and reinforced sand with reinforcement layers of different *G*

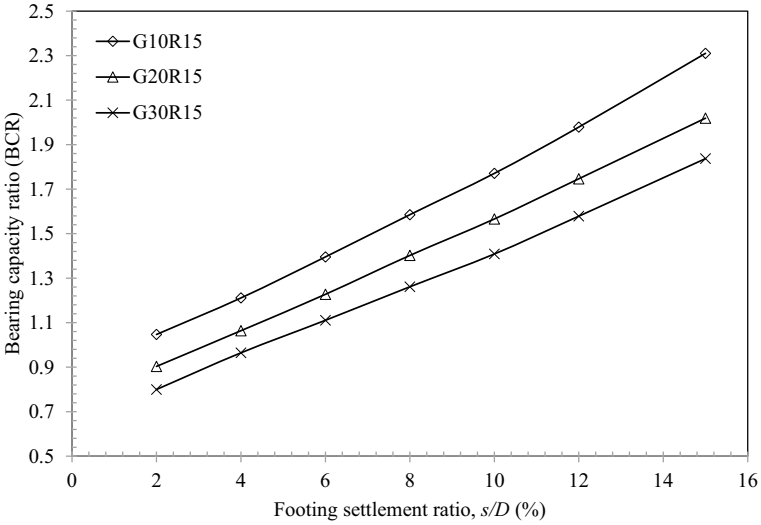

Fig. 9 Variation of BCR with footing settlement (*s/D*) for reinforcements of different *G*

aperture sizes (*G*) of the reinforcement to mobilize a higher tensile bond (consists frictional properties) at the interfaces of sand-grid-geotextile during initial loading. Generally, the soil-reinforcement interface properties are lesser than the unreinforced soil internal frictional properties (Goodhue et al. 2001). As a result, the load-bearing capacity of unreinforced sand is higher than that of reinforced sand during

the first stages of loading. After that, the interface and interlocking properties are mobilized, and the bearing capacity improves more than that of the unreinforced sand bed. Figures 8 and 9 show that the load-carrying capacity was higher for the grid-geotextile with a G of 10 mm × 10 mm (G10R15). This is attributed to the variation in the tensile stiffness of reinforcement material (EA) and $\frac{d_{\min}}{D_{50}}$, where $d_{\min}$ is the minimum dimension of the aperture, and D_{50} is the medium diameter of sand particle size. As observed from Table 2, the tensile stiffness of the grid-geotextiles of G20R15 and G30R15 exhibits low tensile stiffness (EA) compared to the G10R15. Further, Table 2 shows that the ratio of $\frac{d_{\min}}{D_{50}}$ increases with the increase in the aperture size (G). The formation of lateral buckling of soil particles in the geogrids plane along with increasing the geogrid apertures causes a dramatic reduction in BCR (Mehrjardi and Khazaei 2017). Hence, the BCR of the sand bed reinforced with grid-geotextile with G20R15 and G30R15 is lower than that of the sand reinforced with grid-geotextile with G10R15. Irrespective of settlement, the increment of BCR with G10R15 is more than 12 to 22% compared to the reinforcements of G20R15 and G30R15, respectively. Based on this study, it can be concluded that the optimum aperture size for the grid-geotextile is G10R15.

5.2.2 Effect of Rib Size (R)

The previous section shows that the optimum aperture size for the grid-geotextile reinforcement layer is 10 mm × 10 mm (G10R15). To evaluate the effect of the rib width (R) of grid-geotextile, Series D model tests were also performed using grid-geotextiles with G of 10 mm × 10 mm and R of 15 mm (G10R15), 25 mm (G10R25), and 35 mm (G10R35). Figure 10 compares the variation of BCR with the settlement ratio of different rib (R) grid-geotextile–reinforced sand beds. It is clear from Fig. 10 that irrespective of the R, the load-bearing capacity and BCR of the reinforced sand bed increase with an increase in the settlement of the footing (s/D). Further, Fig. 10 depicts that the effect of R has an insignificant bearing on the BCR of the grid-geotextile–reinforced sand. However, the variation of BCR with rib width (R) is presented in Fig. 11.

It is clear from Fig. 11 that the BCR increases with the increase in R and is maximum at the R of G10R25 and beyond which it decreased. However, the percentage increment in BCR of grid-geotextile with G10R25 is 4% and 6% at a settlement ratio of 12% concerning G10R15 and G10R35 rib sizes, respectively. It is attributed to the variation of the tensile stiffness of reinforcement material (EA) and interface and interlocking mechanisms. Table 2 presents that the tensile stiffness of the reinforcement layers (EA) is increasing with the increase in the R. From Table 2 and Fig. 11, there is no relationship between the tensile stiffness of the reinforcement layer and BCR. It means that the BCR of the sand bed reinforced with grid-geotextile reinforcement layer with G10R25 shows higher improvement than the G10R35 reinforcement layer despite the lower tensile stiffness value of G10R25 (Table 2). It should be noted here that the interface frictional resistance increases with the width of the R of grid-geotextile as the G is maintained the same. However, increasing the width R also decreases the number of apertures present per unit area and decreases

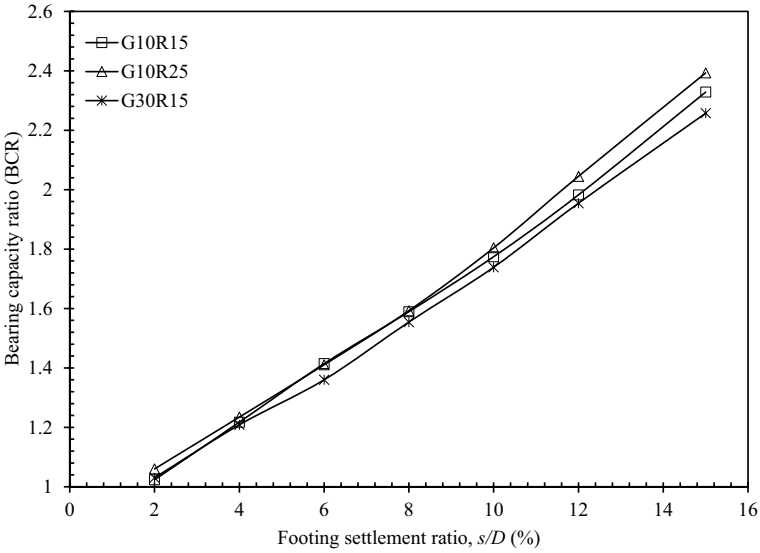

Fig. 10 Variation of the BCR with footing settlement (*s/D*) for reinforcements of different *R*

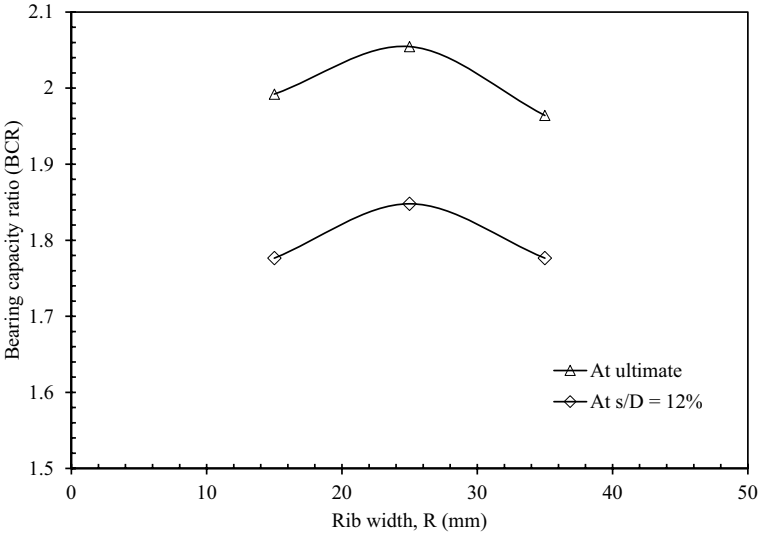

Fig. 11 Comparison of BCR for different rib widths (*R*) of the reinforcement layer

the interlocking contribution. It amounts to say that both interface and interlocking mechanisms play a significant role in the improvement of the load-carrying capacity of the sand bed up to G10R25. Further increase in the *R* from G10R25 to G10R35 decreases the number of apertures in the grid-geotextile reinforcement layer, resulting in the decrease in the interlocking effect and thus the BCR.

5.3 Comparison of Grid-Geotextile with TF–41 and SG–40

Figure 12 shows the variation of BCR of grid-geotextiles with different *R* along with the BCR results of reinforced sand with TF–41 and SG–40. It is evident from Fig. 12 that the improvement of grid-geotextile with aperture size (*G*) of 10 mm × 10 mm and *R* of 25 mm (G10R25) is more significant in comparison with the other reinforcements *R*. Interestingly, the BCR of G10R25 is greater than the BCR of TF–41 despite two times greater tensile strength and stiffness of TF–41, irrespective of the *R*. The percentage increment in BCR of G10R25 is less than 10% at settlement ratio (*s/D*) 12%, and the improvement is greater than 15% at settlement ratios (*s/D*) greater than 12% compared to the BCR of TF–41. This difference mostly happened due to a lack of overburden (i.e., *u/D* and *h/D*) for the case of grid-geotextiles to mobilize maximum interface and interlocking properties during initial loading stages. Hsieh and Mao (2005) also reported that at shallow depths, the efficiency of geotextile reinforcements was slightly higher compared to the geogrid reinforcements improved BCR. However, the load-carrying capacity of the sand bed with SG–40 geogrid reinforcement layers is far greater than the sand reinforced with plane geotextile (TF–41) and grid-geotextile layers, irrespective of aperture and rib sizes. It may be noted here that the aperture size of the SG–40 and G20R15 grid-geotextile reinforcement layers is maintained the same, i.e., 20 × 17 mm (Table 2). Even then, the load-carrying capacity was two-fold higher than the grid-geotextile–reinforced sand at a footing settlement ratio (*s/D*) of 12%. This is due to the higher tensile stiffness property of the SG–40 reinforcement layer (Table 2). The present findings are consistent with the test results reported by Brown et al. (2007).

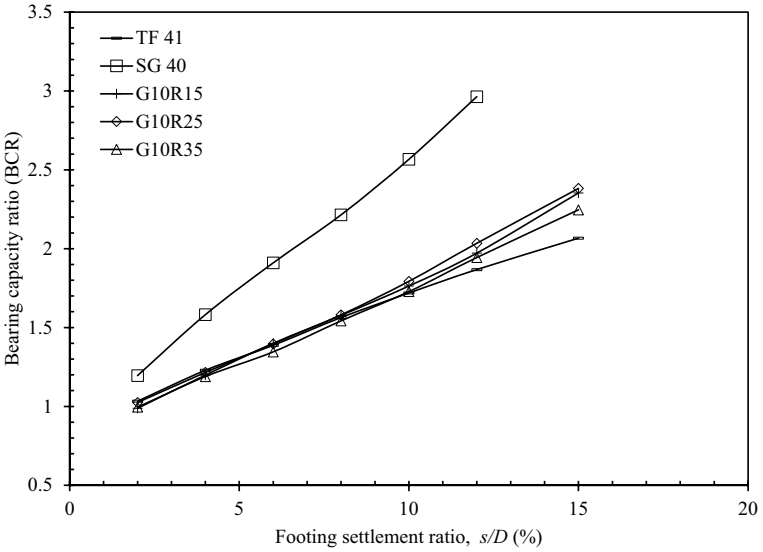

Fig. 12 Variation of the BCR with footing settlement (*s/D*) for reinforced sand with TF–41, SG–40, and grid-geotextiles with different *R*

5.4 Optimum Reinforcement Parameters of $\frac{D}{d_{min}}$, $\frac{D}{D_{50}}$, $\frac{d_{min}}{D_{50}}$

In the case of geogrid-reinforced soils, various parameters influence the soil load-carrying capacity such as the ratio of loading plate size (D) to the minimum dimension of reinforcement aperture ($d_{\min}$), i.e., $\frac{D}{d_{\min}}$; a ratio of loading plate size to the medium soil particle size (D_{50}), i.e., $\frac{D}{D_{50}}$; and $\frac{d_{\min}}{D_{50}}$ (Mehrjardi and Khazaei 2017). These parameters could be optimized for maximum reinforcement efficiency (Brown et al. 2007). With this respect, Fig. 13a, b depicts the variation of BCR of the present study along with the results of various researchers (as per the literature) with different ratios of $\frac{D}{d_{\min}}$. From Fig. 13a, the optimum ratio of loading plate size (D) to minimum aperture dimension of reinforcement ($d_{\min}$) is in the range of 5 to 12.4 (roughly 7.2 on average). It is further confirmed that Fig. 13b shows that various researchers' maximum BCR with different $\frac{D}{d_{\min}}$ falls within the boundary of >5 and <11. It means that the reinforcement consists of smaller grid apertures (i.e., $\frac{D}{d_{\min}} < 11$) and acts as a better reinforcement in soil load-carrying capacity improvement. Moreover, in cases of the same $\frac{D}{d_{\min}}$, Phanikumar et al. (2009) and Demir et al. (2013, 2014) test studies show that the BCR is higher for the smaller medium-sized soil particles (D_{50}). In the case of geogrid-reinforced sands, the beneficial effect of reinforcement was higher at weaker subgrades or backfills (Mehrjardi and Khazaei 2017). Based on this, the effect of soil particles (factor D_{50}) on soil BCR is also considered in terms of $\frac{D}{D_{50}}$ and $\frac{d_{\min}}{D_{50}}$. Figures 14 and 15 present the variation of BCR with different ratios of $\frac{D}{D_{50}}$ and $\frac{d_{\min}}{D_{50}}$. From Figs. 14 and 15, the optimum ranges for the parameters of $\frac{D}{D_{50}}$ and $\frac{d_{\min}}{D_{50}}$ could be 18.8–31.6 (roughly 25 on average) and 3.44–8.235 (approximately 6 on average), respectively.

5.5 Development of Correlations

As per the discussions of the above sections, it is clear that the BCR of the sand bed reinforced with geogrid reinforcement layers mostly depends on the following influencing reinforcement parameters such as EA, $\frac{D}{d_{\min}}$, and $\frac{d_{\min}}{D_{50}}$. Therefore, a simple regression analysis was carried out using the present study test results and the correlations between the reinforcement layer tensile stiffness (EA), a ratio of footing size to the minimum aperture size of reinforcement $\left(\frac{D}{d_{\min}}\right)$, and the ratio of the minimum aperture size to the medium grain size of soil $\left(\frac{d_{\min}}{D_{50}}\right)$. Finally, the correlations for BCR for settlement ratio (s/D) of 10% and ultimate bearing capacity were determined. The regression coefficients of both were found to be 0.98, respectively. The correlations fitted are:

$$BCR = 1.70 - 0.0024\left(\frac{d_{min}}{D_{50}}\right) + 0.0072(EA) + 0.0007\left(\frac{D}{d_{min}}\right) \ (At\ 10\%\ of\ s/D) \tag{1}$$

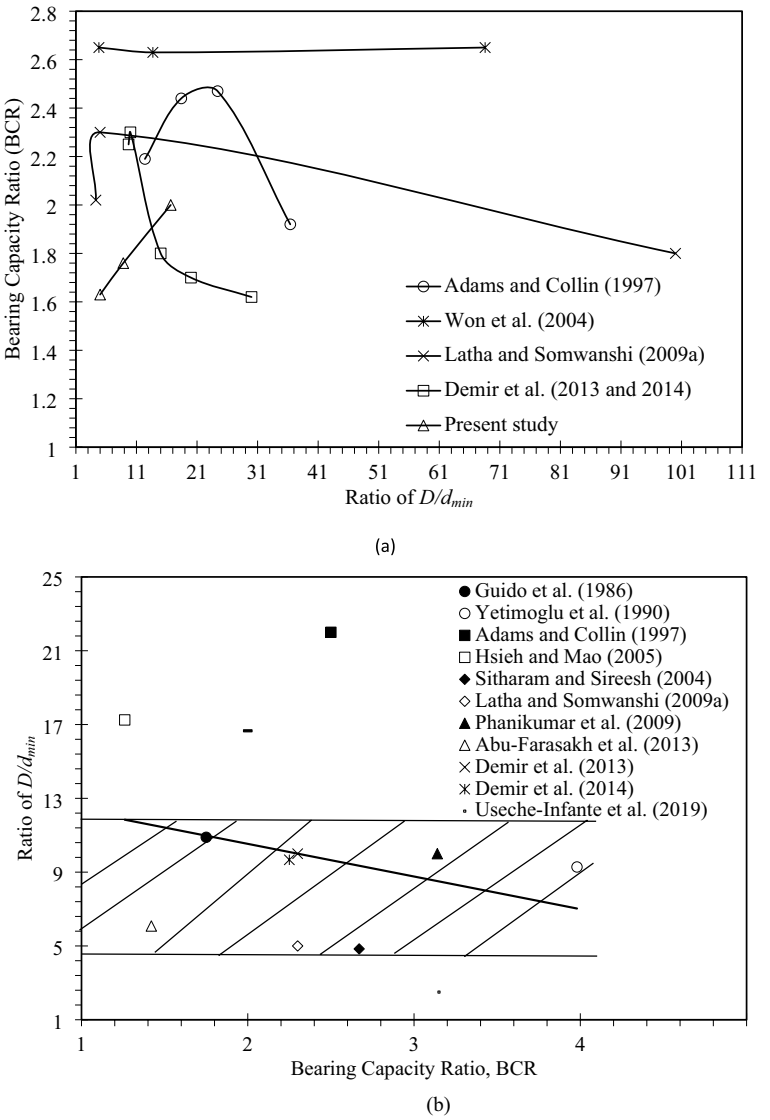

Fig. 13 **a** Comparison of variation of the BCR with different ratios of $\frac{D}{d_{\min}}$, **b** Boundary conditions of $\frac{D}{d_{\min}}$ used by various researchers

$$\mathrm{BCR} = 1.82 - 0.003\left(\frac{d_{\min}}{D_{50}}\right) + 0.0094(EA) - 0.0244\left(\frac{D}{d_{\min}}\right) \text{ (At ultimate)} \quad (2)$$

Generally, shallow foundations are designed to meet serviceability criteria rather than bearing capacity criteria. Hence, the footing settlements are restricted to 10 to 15% of footing size (D) while designing the footings (Tafreshi and

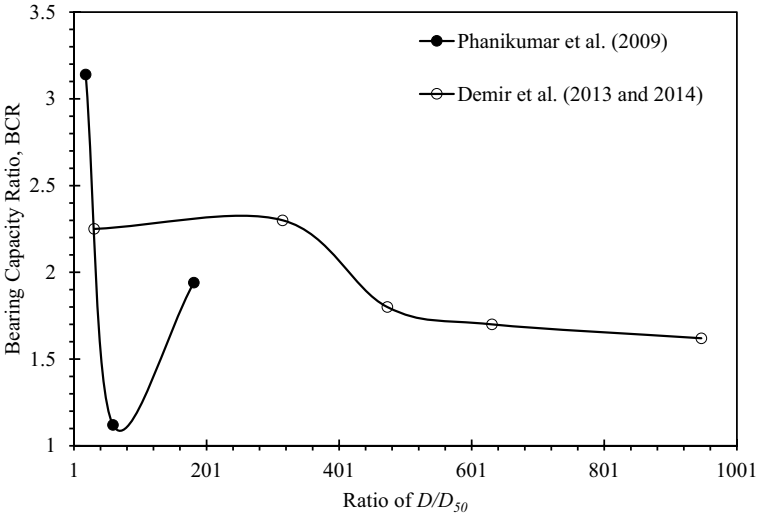

Fig. 14 Comparison of variation of the BCR with different ratios of $\frac{D}{D_{50}}$

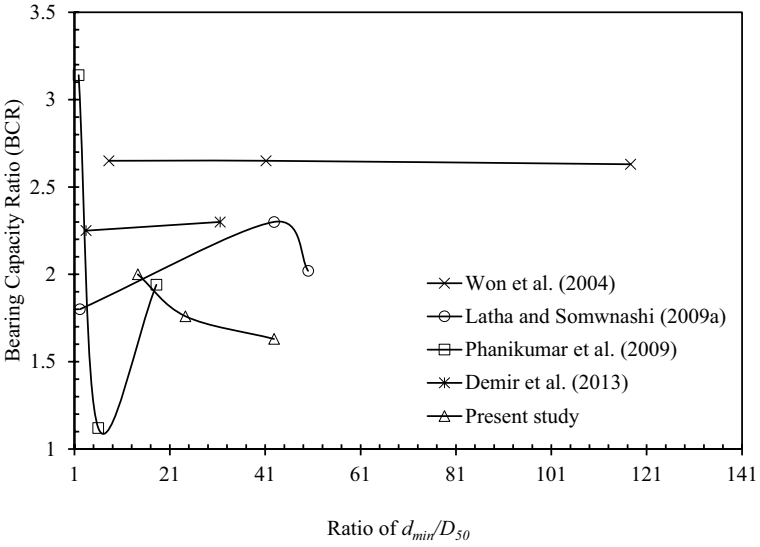

Fig. 15 Comparison of variation of the BCR with different ratios of $\frac{d_{\min}}{D_{50}}$

Dawson 2010). Therefore, the correlations were developed using two different criteria: settlement criterion of 10% and ultimate bearing capacity.

5.6 Validation of Correlations

The correlations obtained from the regression analysis shown in Eqs. 1 and 2 are validated with the available experimental data in the literature. The calculated BCR from the derived correlations and reported BCR in the literature are presented in Table 4. Table 4 also shows the percentage of variation of the BCR from the derived correlations and reported BCR in the literature. While calculating the percentage of variation, the experimental (literature) BCR values are considered actual values for comparison. It can be observed from Table 4 that the variation was much less for tensile stiffness (EA) of the reinforcement layers, less than 250 kN/m, $\frac{D}{d_{\min}}$, and $\frac{d_{\min}}{D_{50}}$ less than 5 and 45. At higher reinforcement tensile stiffness and influencing properties, i.e., EA, $\frac{D}{d_{\min}}$, and $\frac{d_{\min}}{D_{50}}$, the variation was higher as the correlations derived are for the maximum reinforcement tensile stiffness (EA) of 200 kN/m, $\frac{D}{d_{\min}}$, and $\frac{d_{\min}}{D_{50}}$ of 16.667 and 45 (Table 2). Hence, the BCR values calculated from the derived relationships are valid for the sand bed reinforced with geogrid reinforcement layers having properties of tensile stiffness (EA) of less than 200 kN/m, and $\frac{D}{d_{\min}}$ and $\frac{d_{\min}}{D_{50}}$ are between 5–15 and 10–45, respectively.

5.7 Gist of the Matter

The small-scale (1 g and Ng) model tests designed with appropriate scaling laws replicate the actual field prototype footing behavior (Buragadda and Thyagaraj 2019). As per Viswanadham and Konig (2004) and Wood (2004), with a scaling down (N) factor of 2, the present study replicates the behavior of actual concrete structural footing size of 0.68 m having 0.11 m thickness (Buragadda and Thyagaraj 2019). Also, the test results of grid-geotextile–reinforced sand having different apertures represent the reinforced sand in the presence of commercial geogrid reinforcements. As per scale-down factors proposed by Viswanadham and Konig (2004), the model reinforcement physical properties (i.e., thickness and apertures) and mechanical properties (i.e., tensile stiffness) should be lower as N and N^2 times in comparison with the prototype reinforcement properties. For example, from Table 2, the properties of model grid-geotextile G10R25 (EA = 52 kN/m) of the present study represent the behavior of commercial geogrid of SG–40 (EA = 181; nearer to 4 times higher than G10R25). However, in the present study, SG–40 was used only to evaluate the effect of the reinforcement's tensile stiffness (EA) compared with grid-geotextile consisting of the exact aperture sizes on soil load-settlement characteristics (Table 2). Similarly, the behavior of sand with model synthetic polypropylene geotextile TF–41 represents the behavior of sand in the presence of real prototype reinforcement of TechnoFab product named TF–05B. Besides, the ratio of footing size (D) to the medium soil particle size (D_{50}) of the present study is more than 50,

Table 4 Results of bearing capacity ratios (BCR) as obtained from previous researchers' experiments and derived relationships

Author	Type of footing	Size of footing	Type of foundation soil	Type of geogrid reinforcement	Reinforcement *EA*, at 5% strain (kN/m)	Ratio of $\left(\frac{d_{min}}{D_{50}}\right)$	Ratio of $\left(\frac{D}{d_{min}}\right)$	Experimental BCR (at *s/D* of 12%)	Theoretical BCR (at *s/D* of 12%)	Variation (%)	Experimental BCR (at ultimate)	Theoretical BCR (at ultimate)	Variation (%)
Guido et al. (1986)	Square	0.305	Sand	Bi-axial	330**	186.6	10.89	1.75	3.63	107.64	-	-	-
Yetimoglu et al.* (1994)	Rectangular	0.127×0.101	Sand	Bi-axial	238.33	46.66	9.28	3.98	3.31	− 16.94	-	-	-
Adams and Collin* (1997)	Square	0.31	Sand	Bi-axial	450	100	12.4	2.19	4.69	114.59	-	-	-
		0.46					18.4	2.44	4.70	92.76	-	-	-
		0.61					24.4	2.47	4.71	90.58	-	-	-
		0.91					36.4	1.92	4.71	145.59			
Hsieh and Mao* (2005)	Circular	0.30	Sand	Bi-axial	1003.1**	22.01	17.25	1.26	8.85	602.96	-	-	-
Sitharam and Sireesh (2004)	Circular	0.15	Sand	Bi-axial	90.62**	43.75	4.84	2.67	2.25	− 15.70	2.65	2.42	− 8.56
Latha and Somwanshi (2009a)	Square	0.15	Sand	Weak biaxial	160	50	4.29	2.02	2.73	35.24	-	-	-
				Strong biaxial	450	42.86	5	2.3	4.83	109.98	-	-	-
				Geonet	317*	2.14	100	1.8	4.03	12	-	-	-

Table 4 (continued)

Author	Type of footing	Size of footing	Type of foundation soil	Type of geogrid reinforcement	Reinforcement *EA*, at 5% strain (kN/m)	Ratio of $\left(\frac{d_{min}}{D_{50}}\right)$	Ratio of $\left(\frac{D}{d_{min}}\right)$	Experimental BCR (at *s/D* of 12%)	Theoretical BCR (at *s/D* of 12%)	Variation (%)	Experimental BCR (at ultimate)	Theoretical BCR (at ultimate)	Variation (%)
Phanikumar et al. (2009)	Circular	0.06	Sand (coarse)	Biaxial	38.02**	1.88	10	3.14	1.97	−37.07	-	-	-
			Sand (medium)			6.00	10	1.12	1.96	75.53	-	-	-
			Sand (fine)			18.18	10	1.94	1.93	−0.14	-	-	-
Abu-Farsakh et al. (2013)	Square	0.152	Sand	Bi-axial	365	57	6.08	1.63	4.18	156.90	1.42	4.94	248.04
Demir et al. (2013)	Square	0.30	Granular fill	Bi-axial	960	31.57	10	2.3	8.51	270.27	-	-	-
		0.45					15	1.8	8.51	373.30	-	-	-
		0.60					20	1.7	8.52	401.34	-	-	-
		0.90*					30	1.62	8.52	426.50	-	-	-
Demir et al. (2014)	Square	0.30	Granular fill	Bi-axial	960	3.44	9.67	2.25	8.58	281.44	-	-	-
Useche-Infante et al. (2019)	Circular	0.10	Sand	Bi-axial	360	29.17	2.5	3.49	4.21	20.77	3.15	5.06	60.88

*q_{ur} at $s/D < 5\%$

**EA at ultimate failure strain, i.e., > 5% or < 5%

so the influence of soil particle sizes on prototype footing load-settlement characteristics is insignificant (Toyosawa et al. 2013).

6 Summary and Conclusions

In this study, the plate load tests were performed on unreinforced sand beds (URS) and reinforced sand beds using plane geotextile (TF–41), grid-geotextiles consisting of different aperture (G) and rib (R) sizes, and biaxial geogrid reinforcement layers (SG–40). Based on the test results, the following conclusions have been drawn:

(1) The improvement in the load-carrying capacity of the sand bed reinforced with four-layered TF–41 reinforcement layers was 1.8 times greater than the URS. However, the improvement with SG–40 was almost three times greater than the URS and 1.2 times greater than the TF–41-reinforced sand bed at a footing settlement ratio (s/D) of 12%.
(2) The grid-geotextile G10R15 showed two times higher load-carrying capacity improvement compared to the G20R15 and G30R15 grid-geotextile–reinforced sand beds.
(3) The grid-geotextile G10R25 showed more significant improvement than the grid-geotextiles with G10R15 and G10R35. Irrespective of the R, the grid-geotextile layers' tensile strength and stiffness were 2 times lower than the TF–41. However, the percentage increment of grid-geotextile sand bed was less than 10% at a footing settlement ratio (s/D) less than 12% and more than 15% at a footing settlement ratio (s/D) greater than 12% as compared with the sand reinforced with high tensile strength TF–41.
(4) Due to the high tensile stiffness property of SG–40, the improvement in the load-carrying capacity of the sand bed reinforced with geogrid reinforcement layers is significant in comparison to the grid-geotextile–reinforced sand bed even with the same aperture size of G20R15.
(5) The test results reveal that the minimum dimension of the aperture size (d_{min}) should be around 0.2 times the footing width (D). Similarly, the optimum size of the loading plate (D) and the maximum dimension (d_{min}) of the aperture size of the reinforcement should respectively be around 25 times and 6 times as compared to the medium size of soil particles (D_{50}).
(6) The correlations are developed for the finding of BCR of the reinforced sand bed with variable parameters of tensile stiffness of geogrid reinforcement (EA) and the ratios of the $\frac{D}{d_{\text{min}}}$ and $\frac{d_{\text{min}}}{D_{50}}$. The developed correlations are valid for the sand beds reinforced with geogrid reinforcement layers with tensile stiffness (EA) values of less than 200 kN/m, and $\frac{D}{d_{\text{min}}}$ and $\frac{d_{\text{min}}}{D_{50}}$ are between 5–15 and 10–45, respectively.

Nomenclature B_r: Width of the reinforcement layer (mm); C_c: Soil particles curvature coefficient (dimensionless); C_u: Soil particle's uniformity coefficient (dimensionless); CMD: Cross-machine direction; D: Diameter of the footing (mm); D_{50}: Medium soil particle size (mm); d_{min}: Minimum dimension of apertures (mm); G: Aperture size of grid-geotextile (mm); h: Vertical spacing of the reinforcement layers (mm); MD: Machine direction; N: Number of reinforcement layers; q_r: Load-bearing pressure (kPa); q_{us}: Unreinforced sand load-bearing capacity at a footing settlement of "s" (kPa); q_{uult}: Unreinforced sand ultimate load-bearing capacity (kPa); q_{rs}: Reinforced sand load-bearing capacity at a footing settlement of "s" (kPa); q_{rult}: Reinforced sand ultimate load-bearing capacity (kPa); R: Rib size of grid-geotextile (mm); R_d: Relative density of sand (%); s: Footing settlement (mm); SG: Strata Grid; TF: Techno Fabric; u: Placement depth of the top reinforcement layer from the footing base (mm); URS: Unreinforced sand load-carrying capacity (kPa)

Author Contribution Venkatesh Buragadda and Eswara Reddy Orekanti conceptualized, designed, and carried out the experiments, analyzed the results, and contributed to writing the original draft preparation. Thyagaraj, T. and Rishav Dhiman were instrumental during conceptualization, initial design, and reviewing. Tharun Kumar Maddileti contributed to analyzing the results and contributed to writing, reviewing, and editing.

Funding This research did not receive any specific grant from funding agencies in the public, commercial, or not-for-profit sectors.

Data Availability All data, models, and code generated or used during the study appear in the published article.

Code Availability Not applicable.

Declarations

Ethics Approval and Consent to Participate Not applicable.

Consent for Publication Not applicable.

Competing Interests The authors declare no competing interests.

References

Abu-Farsakh, M., Chen, Q., Sharma, R.: An experimental evaluation of the behavior of footings on geosynthetic-reinforced sand. Soils Foundations **53**(2), 335–348 (2013). https://doi.org/10.1016/j.sandf.2013.01.001

Adams, M.T., Collin, J.G.: Large model spread footing load tests on geosynthetic reinforced soil foundations. J. Geotech. Geoenviron. Eng. **123**(1), 66–72 (1997). https://doi.org/10.1061/(ASCE)1090-0241(1997)123:1(66)

ASTM D 4595–17: Standard test method for tensile properties of geotextiles by the wide-width strip method. ASTM Int, West Conshohocken (2017)

ASTM D 5199–12: Standard test method for measuring the nominal thickness of geosynthetics. ASTM Int, West Conshohocken (2012)

ASTM D 5261–10: Standard test method for measuring mass per unit area of geotextiles. ASTM Int, West Conshohocken (2018)

ASTM D 6637: Standard test method for determining tensile properties of geogrids by the single or multi-rib tensile method. ASTM Int, West Conshohocken (2015)

ASTM D6913: Standard test methods for particle-size distribution (gradation) of soils using sieve analysis. ASTM Int, West Conshohocken (2017)

Brown, S.F., Kwan, J.N., Thom, H.: Identifying the key parameters that influence geogrid reinforcement of railway ballast. Geotextiles Geomembr. **25**(6), 326–335 (2007). https://doi.org/10.1016/j.geotexmem.2007.06.003

Buragadda, V., Thyagaraj, T.: Bearing capacity of jute geotextile-reinforced sand bed. Int. J. Geosynth. Ground Eng. **5**(4), 1–14 (2019). https://doi.org/10.1007/s40891-019-0178-6

Demir, A., Laman, M., Yildiz, A., Ornek, M.: Large scale field tests on geogrid-reinforced granular fill underlain by clay soil. Geotextiles Geomembr. **38**, 1–15 (2013). https://doi.org/10.1016/j.geotexmem.2012.05.007

Demir, A., Yildiz, A., Laman, M., Ornek, M.: Experimental and numerical analyses of circular footing on geogrid-reinforced granular fill underlain by soft clay. Acta Geotech. **9**(4), 711–723 (2014). https://doi.org/10.1007/s11440-013-0207-x

Gongora, I.A., Palmeira, E.M.: Assessing the influence of soil-reinforcement interaction parameters on the performance of a low fill on compressible subgrade. Part II: influence of surface maintenance. Int. J. Geosynth. Ground Eng. **2**(1), 2 (2016). https://doi.org/10.1007/s40891-015-0042-2

Goodhue, M.J., Edil, T.B., Benson, C.H.: Interaction of foundry sands with geosynthetics. J. Geotech. Geoenviron. Eng. **127**(4), 353–362 (2001). https://doi.org/10.1061/(ASCE)1090-0241(2001)127:4(353)

Guido, V.A., Chang, D.K., Sweeney, M.A.: Comparison of geogrid and geotextile reinforced earth slabs. Can. Geotech. J. **23**(1), 435–440 (1986). https://doi.org/10.1139/t86-073

Guo, X., Zhang, H., Liu, L.: Planar geosynthetic-reinforced soil foundations: a review. SN Appl. Sci. **2**(12), 1–18 (2020). https://doi.org/10.1007/s42452-020-03930-5

Hsieh, C., Mao, H. L. A bench-scale performance test for evaluation the geosynthetic reinforcement effects on granular base courses. In: GRI-18 Geosynthetics Research and Development in Progress. Geofrontiers, Austin (2005) https://doi.org/10.1061/40782(161)9

IS: 1888: Method of load test on soils. Bureau of Indian Standards, New Delhi (1982)

Latha, G.M., Somwanshi, A.: Bearing capacity of square footings on geosynthetic reinforced sand. Geotextiles Geomembr. **27**(4), 281–294 (2009a). https://doi.org/10.1016/j.geotexmem.2009.02.001

Latha, G.M., Somwanshi, A.: Effect of reinforcement form on the bearing capacity of square footings on sand. Geotextiles Geomembr. **27**(6), 409–422 (2009b). https://doi.org/10.1016/j.geotexmem.2009.03.005

Mehrjardi, G.T., Khazaei, M.: Scale effect on the behaviour of geogrid-reinforced soil under repeated loads. Geotextiles Geomembr. **45**(6), 603–615 (2017). https://doi.org/10.1016/j.geotexmem.2017.08.002

Omar, M.T., Das, B.M., Puri, V.K., Yen, S.C.: Ultimate bearing capacity of shallow foundations on sand with geogrid reinforcement. Can. Geotech. J. **30**(3), 545–549 (1993). https://doi.org/10.1139/t93-046

Phanikumar, B.R., Prasad, R., Singh, A.: Compressive load response of geogrid-reinforced fine, medium and coarse sands. Geotextiles Geomembr. **27**(3), 183–186 (2009). https://doi.org/10.1016/j.geotexmem.2008.11.003

Shukla, S., Sivakugan, N., Das, B.: Fundamental concepts of soil reinforcement - an overview. Int. J. Geotech. Eng. **3**(3), 329–342 (2009). https://doi.org/10.3328/IJGE.2009.03.03.329-342

Sitharam, T.G., Sireesh, S.: Model studies of embedded circular footing on geogrid-reinforced sand beds. Ground Improve. **8**(2), 69–75 (2004). https://doi.org/10.1680/grim.2004.8.2.69

Tafreshi, S.M., Dawson, A.R.: Comparison of bearing capacity of a strip footing on sand with geocell and with planar forms of geotextile reinforcement. Geotextiles Geomembr. **28**(1), 72–84 (2010). https://doi.org/10.1016/j.geotexmem.2009.09.003

Toyosawa, Y., Itoh, K., Kikkawa, N., Yang, J.J., Liu, F.: Influence of model footing diameter and embedded depth on particle size effect in centrifugal bearing capacity tests. Soils Foundations **53**(2), 349–356 (2013). https://doi.org/10.1016/j.sandf.2012.11.027

Useche-Infante, D., Aiassa Martine, G., Arrúa, P., Eberhardt, M.: Experimental study of the behaviour of circular footing on geogrid-reinforced sand. Geomech. Geoeng. 1–19 (2019). https://doi.org/10.1080/17486025.2019.1683621

Viswanadham, B.V.S., Konig, D.: Studies on scaling and instrumentation of a geogrid. Geotextiles Geomembr. **22**(5), 307–328 (2004). https://doi.org/10.1016/S0266-1144(03)00045-1

Wood, D.M.: Geotechnical modelling. Taylor & Francis (2004)

Yetimoglu, T., Wu, J.T.H., Saglamer, A.: Bearing capacity of rectangular footings on geogrid-reinforced sand. J. Geotech. Eng. **120**(12), 2083–2099 (1994). https://doi.org/10.1061/(ASCE)0733-9410(1994)120:12(2083)

Authors and Affiliations

Venkatesh Buragadda[1,3] · T. Thyagaraj[2] · Rishav Dhiman[2] · Eswara Reddy Orekanti[1] · Tharun Kumar Maddileti[1]

✉ Venkatesh Buragadda
venkateshiitm15@gmail.com

T. Thyagaraj
ttraj@smail.iitm.ac.in

Rishav Dhiman
rishav.dhiman89@gmail.com

Eswara Reddy Orekanti
orekantieswar@gmail.com

Tharun Kumar Maddileti
iamtharun.m@gmail.com

[1] Department of Civil Engineering, School of Engineering, Mohan Babu University (Erstwhile Sree Vidyanikethan Engineering College), Tirupati, Andhra Pradesh 517102, India

[2] Geotechnical Engineering Division, Department of Civil Engineering, Indian Institute of Technology Madras, Chennai 600036, Tamil Nadu, India

[3] Faculty of Engineering and Built Environment, School of Civil and Environmental Engineering, University of the Witwatersrand, Johannesburg, South Africa